Rates of Unfolding, Rather than Refolding, Determine Thermal Stabilities of Thermophilic, Mesophilic, and Psychrotrophic 3-Isopropylmalate Dehydrogenases†

Éva Gráczer,[‡,||] Andrea Varga,[‡,||] István Hajdú,[‡] Bogdan Melnik,[§] András Szilágyi,[‡] Gennady Semisotnov,[§] Péter Závodszky,[‡] and Mária Vas*[,‡]

Institute of Enzymology, Biological Research Center, Hungarian Academy of Sciences, P.O. Box 7, H-1518 Budapest, Hungary, and Institute of Protein Research, Russian Academy of Sciences, 142290 Pushchino, Moscow Region, Russia

Received April 20, 2007; Revised Manuscript Received August 3, 2007

ABSTRACT: The relationship between the thermal stability of proteins and rates of unfolding and refolding is still an open issue. The data are very scarce, especially for proteins with complex structure. Here, time-dependent denaturation−renaturation experiments on *Thermus thermophilus*, *Escherichia coli*, and *Vibrio* sp. I5 3-isopropylmalate dehydrogenases (IPMDHs) of different heat stabilities are presented. Unfolding, as monitored by several methods, occurs in a single first-order step with half-times of ∼1 h, several minutes, and few seconds for the thermophilic, mesophilic, and psychrotrophic enzymes, respectively. The binding of Mn*IPM (the manganese complex of 3-isopropylmalate) markedly reduces the rates of unfolding; this effect is more prominent for the less stable enzyme variants. Refolding is a two-step or multistep first-order process involving an inactive intermediate(s). The restoration of the native structure and reactivation take place with a half-time of a few minutes for all three IPMDHs. Thus, the comparative experimental unfolding−refolding studies of the three IPMDHs with different thermostabilities have revealed a close relationship between thermostability and unfolding rate. Structural analysis has shown that the differences in the molecular contacts between selected nonconserved residues are responsible for the different rates of unfolding. On the other hand, the folding rates might be correlated with the absolute contact order, which does not significantly vary between IPMDHs with different thermostabilities. On the basis of our observations, folding rates appear to be dictated by global structural characteristics (such as native topology, i.e., contact order) rather than by thermodynamic stability.

The mechanism of evolutionary adaptation of proteins to various environmental temperatures is still debated (*1*−*8*). Most studies comparing proteins adapted to different temperatures, such as those from thermophilic, mesophilic, and psychrophilic sources, have focused on the structural differences, which are generally very subtle between orthologous proteins. Various structural properties (e.g., hydrogen bond content, number of salt bridges, core packing, length of surface loops) can be correlated with thermal stability (*2*, *6*, *8*−*11*). Studies comparing the rates and kinetic mechanisms of unfolding and refolding of proteins adapted to various temperatures are also needed. Kinetic parameters can be obtained from time-dependent denaturation−renaturation studies and can provide information about the dynamics of protein stabilization mechanisms and the presence of a kinetic intermediate(s). Unfolding−refolding studies can also contribute to our understanding of the mechanisms of protein folding in general.

Until now, kinetic and thermodynamic studies with proteins of different heat stabilities have mostly been restricted to single-domain or monomeric proteins (e.g., refs *12*−*17*). Data for multidomain or oligomeric proteins are very scarce (e.g., ref *18*). Studies are often hampered by the irreversibility of unfolding, especially in the case of complex protein structures (cf. ref *4*).

Experimental studies so far have not provided evidence of a general correlation between unfolding or refolding rates and protein stability. While theoretical studies suggested that protein stability should influence the rate and mechanism of folding (*19*−*23*), experimental results are equivocal. One set of data shows a linear correlation between stability and folding rate (*15*, *24*−*28*), while another set of data shows a correlation between stability and unfolding rate, and no link between stability and folding rate (*12*−*14*, *17*, *18*). There is also an example in which neither the folding rate nor the unfolding rate varies with thermostability (*16*). To clarify this point and to reach more general conclusions, further data

† This work has been prepared in the framework of the Hungarian-Russian Intergovernmental Scientific and Technological Cooperation Program and was supported by a grant (OMFB-00757/2005, Project RUS-15/04) from the Hungarian Foundation of Research and Innovative Technology as well as by the Ministry of Politics of Science and Technology of the Russian Federation. The financial support provided by Grants OTKA T 043446, 046412, and NI 61915 from the Hungarian National Research Foundation as well as Grant GVOP-3.2.1. 2004-04 0195/3.0, HHMI Grant N-55005607, and the MCB program of the Russian Academy of Sciences (Grant 10002-251/II/145-161/140503-089 and RFBR Grant 06-04-48955) is also gratefully acknowledged. A.S. was supported by a Bolyai János fellowship.

* To whom correspondence should be addressed: Institute of Enzymology, BRC, Hungarian Academy of Sciences, H-1518 Budapest, P.O. Box 7, Hungary. Telephone: 36 1 279 3152. Fax: 36 1 466 5465. E-mail: vas@enzim.hu.

‡ Hungarian Academy of Sciences.

§ Russian Academy of Sciences.

|| These authors contributed equally to this work.

10.1021/bi700754q CCC: $37.00
Published on Web 09/22/2007

for reversibly denaturing proteins of different heat stabilities are needed.

In this work, we describe comparative unfolding−refolding kinetic studies with variants of a dimeric two-domain protein, the enzyme 3-isopropylmalate dehydrogenase (IPMDH),[1] exhibiting different heat stabilities. IPMDH catalyzes the oxidative decarboxylation of threo-D-3-isopropylmalate (IPM) to 2-oxoisocaproate using NAD and a divalent cation (Mn^{2+} or Mg^{2+}) as cofactors. The variants of IPMDH we investigated are from three bacteria, the thermophilic *Thermus thermophilus* (Tt), the mesophilic *Escherichia coli* (Ec), and the psychrotrophic *Vibrio* sp. I5 (Vib) (an organism living in the Arctic Sea; cf. ref *29*). These IPMDHs have been extensively used to investigate the mechanism of thermal adaptation in structural and equilibrium unfolding−refolding studies (*9*, *10*, *30*−*41*). Crystal structures of Tt (*42*, *43*) and Ec IPMDHs (*44*), among others (*44*−*46*), are known and show a peculiar mode of association of the two subunits with the aid of two interacting arms. No crystal structure of Vib IPMDH has been determined, but a homology model was constructed using the structure of Tt, Ec, and *Salmonella typhimurium* enzymes (*10*). Figure 1A depicts the three-dimensional structure of an IPMDH subunit, and Figure 1B shows the aligned primary sequences of Tt, Tf, Ec, and Vib IPMDHs.

The dimeric structure of IPMDHs is of special interest because the binding site of the substrate, IPM, is formed by side chains from both subunits (*44*−*46*). It follows, therefore, that only the dimer may possess enzyme activity. Previous equilibrium denaturation (*33*) and calorimetric (*30*) studies suggested the presence of a dimeric intermediate during the folding process, but kinetic unfolding−refolding studies have not yet been performed with this reversibly denaturing enzyme.

The aim of this work is to identity similarities and/or differences between the time courses of unfolding and refolding processes of the three IPMDHs and to relate these characteristics to the different heat stabilities of these proteins and to their individual structural parameters such as contact order, chain length, and sequence conservation.

MATERIALS AND METHODS

Reagents. Threo-DL-3-isopropylmalic acid (IPM) was purchased form Wako Biochemicals. NAD and NADH were Boehringer Mannheim products. Ellman's reagent (Nbs_2) was obtained from Serva. Isopropyl 1-thio-β-D-galactopyranoside (IPTG) (Fermentas), chloramphenicol, and ampicillin (Sigma) were used for fermentation. Chromatography media were obtained from GE Healthcare. All other chemicals (high purity grade) were products of Merck, Reanal, and Sigma.

Enzyme Expression and Purification. The non-His-tagged variants of Tt and Vib IPMDHs were produced in Ec OM17 cells by expression of plasmids pUTL118 (*47*) and pGWII (*10*) with the Tt leuB and Vib gene, respectively. The His-tagged variants of Tt and Ec IPMDHs (containing the additional AS- sequence at the N-terminus and the -AAALE-HHHHHH sequences at the C-terminus) were also constructed, providing a simpler purification procedure. In this case, the protein synthesis was carried out in BL21(DE3) LysS Ec cells containing the pET21c plasmid carrying the appropriate IPMDH gene. Both OM17 and BL21 Ec cells were grown at 37 °C in the presence of 100 μg/mL ampicillin, and for the BL21 cells, 30 μg/mL chloramphenicol was also used. IPMDH gene expression was induced with 0.4 mM IPTG.

The purification of the non-His-tagged variant of Tt IPMDH was based on the method of Yamada et al. (*48*) with a slight modification by Svingor et al. (*36*). The same method was applied also for isolation of Vib IPMDH.

The His-tagged variants of the Tt and Ec IPMDHs were purified using Ni^{+} affinity chromatography. The bound IPMDHs were eluted at 120 mM imidazole. In all cases, the collected protein fractions were dialyzed against 20 mM KH_2PO_4-KOH buffer (pH 7.6). For Ec and Vib IPMDH, the dialysis buffer contained also 1 mM DTT. The purity of IPMDHs was tested by SDS−PAGE stained with Coomassie Brilliant Blue, where single bands were observed. It was determined that the His-tag attached to Tt IPMDH did not affect either the enzymatic properties or the unfolding−refolding processes. This allowed us to carry out comparative studies with His-tagged Ec and non-His-tagged Vib IPMDHs, too. The dialyzed enzyme solutions were frozen in liquid nitrogen and stored at −80 °C.

Determination of Protein Concentrations and Enzyme Activities. Protein concentrations were determined from the UV absorption at 280 nm. The molar absorption coefficients of 47 900 M^{-1} cm^{-1} for Tt IPMDH and 54 780 M^{-1} cm^{-1} for Ec or Vib IPMDH, respectively, are calculated for the dimers from the amino acid contents using the formula given by Pace and co-workers (*49*). The molecular masses of the non-His-tagged variants of Tt, Ec, and Vib IPMDHs were taken to be 73 300, 78 780, and 76 960 Da, respectively. The His tag caused an additional increase in all molecular masses of 1430 Da.

The activity of IPMDH (6−12 μg/mL, i.e., 0.08−0.16 μM) was assayed in the presence of 0.25 mM IPM, 0.35 mM $MnCl_2$, and 1.3 mM NAD in 20 mM KH_2PO_4-KOH buffer (pH 7.6) containing 300 mM KCl and 10 mM DTT. The formation of NADH was recorded spectrophotometrically at 340 nm. The measurements were carried out at 20 °C using a Jasco (Tokyo, Japan) V-550 spectrophotometer equipped with a Grant Y6 thermostat. The molar activities of Tt, Ec, and Vib IPMDHs were 450 ± 50, 1400 ± 150, and 1600 ± 150 min^{-1}, respectively.

Unfolding and Refolding Experiments. Denaturation of IPMDH was carried out in a solution containing 8.5 M urea, 20 mM KH_2PO_4-KOH buffer (pH 7.6), 300 mM KCl, and 10 mM DTT. It was determined that omission of KCl from the buffer did not influence the experimental results. The concentration of IPMDHs in the denaturation experiments varied from 12 to 100 μg/mL (from 0.16 to 1.36 μM, dimer concentrations). For renaturation studies, denatured Tt, Ec, or Vib IPMDHs were prepared at much higher protein concentrations (usually 600 μg/mL, i.e., 8.15 μM) upon incubation in 8.5 M urea for 24 h, 1 h, or 10 min, respectively, in order to reach complete denaturation. Refolding experiments were initiated by 10−100-fold dilution of

[1] Abbreviations: Tt, *Thermus thermophilus*; Ec, *Escherichia coli*; Vib, *Vibrio* sp. I5; Tf, *Thiobacillus ferrooxidans*; IPMDH, 3-isopropylmalate dehydrogenase; IPM, threo-D-3-isopropylmalate; IPTG, isopropyl 1-thio-β-D-galactopyranoside; ANS, 1-anilinonaphthalene-8-sulfonic acid; Nbs_2, Ellman's reagent [5,5′-dithiobis(2-nitrobenzoic acid)]; CO, contact order.

A

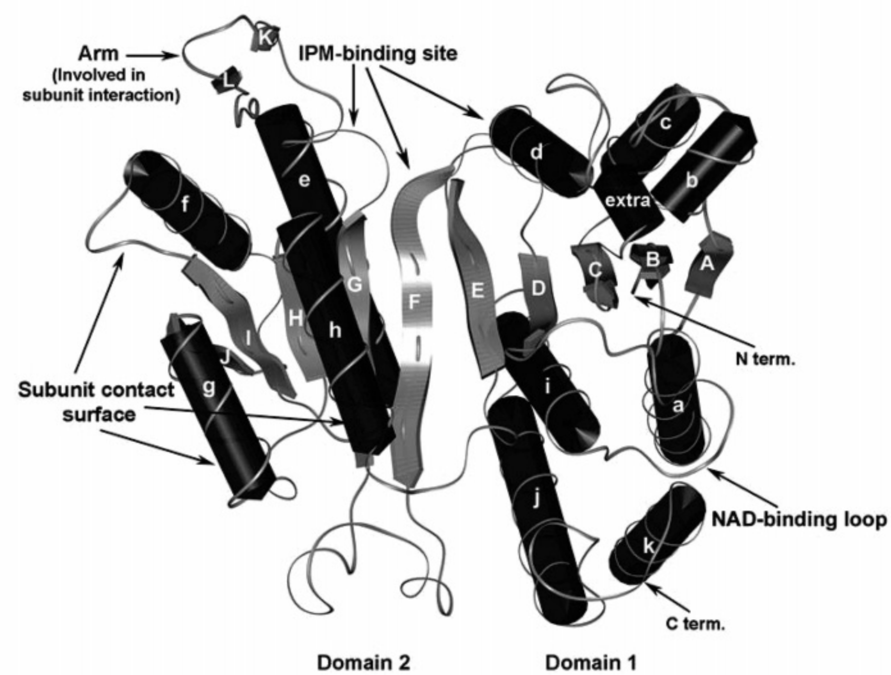

B

```
                βB                αa                 βA          αb             αc        βC
Tt    1     MKVAVL PGDGIGPEVT EAALKVLRAL DEAEGLGLAY EVFPFGGAAI DAFGEPFPEP TRKGVEEAEA 66
Tf    1    MKKIAIF AGDGIGPEIV AAARQVLDAV DQAAHLGLRC TEGLVGGAAL DASDDPLPAA SLQLAMAADA 67
Ec    1 MSKNYHIAVL PGDGIGPEVM TQALKVLDAV RNRFAMRITT SHYDVGGAAI DNHGQPLPPA TVEGCEQADA 70
Vib   1   MSNQILIL PGDGIGPEIM AEAVKVLNLA NEKYSLGFEL SFDDLGGAAI DRYGVPLADE TLARAKAADA 68
                    ** * *                               *                        *

         βC       extra             αd              βF                            βG
Tt   67 VLLGSVGGPK WDGLPRKISP ETG-LLSLRK SQDLFANLRP AKVFPGLERL SPLKEEIARG -VDVLIVREL 134
Tf   68 VILGAVGGPR WDAYPPAKRP EQG-LLRLRK GLDLYANLRP AQIFPQLLDA SPLRPELVRD -VDILVVREL 135
Ec   71 VLFGSVGGPK WEHLPPDQQP ERGALLPLRK HFKLFSNLRP AKLYQGLEAF CPLRADIAAN GFDILCVREL 140
Vib  69 ILLGAVGGPK WDAIDPAIRP ERG-LLKIRS QLGLFGNLRP AILYPQLADA SSLKREIVAG -LDILIVREL 136
              *               *   **  *        * **                               **
              *               *   **  *          *                               *

                   βK              βL             αe               βI              αf
Tt  135 TGGIYFGEPR -GMS--E--A EAWNTERYSK PEVERVARVA FEAARKRRKH VVSVDKANVL EVGEFWRKTV 199
Tf  136 TGDIYFGQPR -GLEVIDGKR RGFNTMVYDE DEIRRIAHVA FRAAQGRRKQ LCSVDKANVL ETTRLWREVV 204
Ec  141 TGGIYFGQPK -GREGSGQYE KAFDTEVYHR FEIERIARIA FESARKRRHK VTSIDKANVL QSSILWREIV 209
Vib 137 TGGIYFGQPR ESKVLESGER MAYDTLPYSE SEIRRIARVG FDMARVRGKK LCSVDKANVL ASSQLWRTVV 206
            *                        *    *  *         *  *         * **       *
            *                                                       *  *

          αf         βJ        αg             βH           αh                βE          βD
Tt  200 EEVGRGYPDV ALEHQYVDAA AMHLVRSPAR FDVVVTGNIF GDILSDLASV LPGSLGLLPS ASLG-RGTPV 268
Tf  205 TEVARDYPDV RLSHMYVDNA AMQLIRAPAQ FDVLLTGNMF GDILSDEASQ LTGSIGMLPS ASLGE-GRAM 273
Ec  210 NEIATEYPDV ELAHMYIDNA TMQLIKDPSQ FDVLLCSNLF GDILSDECAM ITGSMGMLPS ASLNEQGFGL 279
Vib 207 IEVAKDYPDV ELSHMYVDNA AMQLVRAPKQ FDVMVTDNLF GDILSDEASM LTGSIGMLPS ASLDANNKGM 276
                          *    *     *          * * **   *       *  *   *
                          *                          *                *

         βD                        αi                     αj
Tt  269 FEPVHGSAPD IAGKGIANPT AAILSAAMML EHAFGLVELA RKVEDAVAKA LLE-TP-PPD LG--G--SAG 332
Tf  274 YEPIHGSAPD IAGQDKANPL ATILSVAMML RHSLNAEPWA QRVEAAVQRV LDQGL-RTAD IAAPGTPVIG 342
Ec  280 YEPAGGSAPD IAGKNIANPI AQILSLALLL RYSLDADDAA CAIERAINRA LEEGI-RTG- DLARGAAAVS 347
Vib 277 YEPCHGSAPD IAGQGIANPL ATILSVSMML RYSFNQTAAA DAIELAVSNV LDQGL-RTGD IYSAGTTKVG 345
         **  *****         *      *
             *****

              αk
Tt  333 TEAFTATVLR HLA 345
Tf  343 TKAMGAAVVN ALNLKD 358
Ec  348 TDEMGDIIAR YVAEGV 363
Vib 346 TTAMGDAVVE ALRSL 360
```

FIGURE 1: Three-dimensional structure-based sequence alignment of IPMDHs from different origins. (A) Illustration of a single subunit of IPMDH as exemplified by the structure of the Tt enzyme (*52*), showing the arrangement and labeling of the various secondary structure elements (according to ref *42*). (B) Alignment of IPMDH sequences by the corresponding secondary structure elements of Tt with Ec and Vib IPMDHs using molecular graphics. The sequence of Tf IPMDH, with bound Mn*IPM in the crystal structure (*42*), is also included. The selected 46 conserved residues (cf. Materials and Methods) are marked with a single asterisk. An additional asterisk marks the 18 residues that directly interact with the substrates (11 residues with IPM and eight residues with NAD, one of them interacting with both substrates). The locations of secondary structure elements are labeled with arrows.

the denatured protein into the same phosphate buffer described above. The final protein concentration of the renaturation mixtures varied from 6 to 120 μg/mL (i.e., from 0.08 to 1.63 μM). Time courses of unfolding and refolding were followed at 20 °C by various methods as described below. All the experiments were carried out both in the absence and in the presence of substrates. In the latter case, the binary complexes with IPM, Mn*IPM, NAD, or NADH and the ternary complexes with Mn*IPM and NAD or Mn*IPM and NADH were investigated. All substrates were present at the concentrations given in the activity assay mixture. NADH was applied at the same concentration as NAD.

The extent of refolding varied between 50 and 70% for all three enzymes in a manner independent of methods used for detection and of the presence of substrates.

Circular Dichroism Measurements. CD measurements were performed on a Jasco J-720 spectropolarimeter equipped with a Neslab RTE 111 computer-controlled thermostat. Spectra and time courses of denaturation and renaturation were measured using the cuvettes with path lengths of 0.1, 1, or 10 mm, in the order of decreasing protein concentration. The unfolding−refolding kinetic experiments were performed by monitoring the changes in ellipticity at 225 nm.

Protein Fluorescence Measurements. The changes in protein fluorescence during the urea-induced unfolding and refolding were recorded using a SPEX (Edison, NJ) Fluoromax-3 spectrofluorimeter equipped with a Peltier thermostat. The samples were excited at 275 nm, and the emission was monitored at 335 nm using the cuvette with a 10 mm path length. The slits of 2 nm and 2 or 4 nm were applied for excitation and emission, respectively, depending on the actual protein concentration.

Test of Enzyme Activity during Unfolding and Refolding. The time course of activity loss during denaturation was determined by taking aliquots from the denaturation mixture at various time intervals. These samples were diluted 60−110-fold into separate activity assay mixtures, and the activities were determined from the initial slope of the activity curves, considering only the first 5−10 s of the measurements. This way, the reactivation occurring in the activity assay mixture did not perturb the measurements. The time course of protein reactivation during refolding was obtained by withdrawing aliquots at different times from the renaturation mixture, and their activities were assayed as described above.

Following Unfolding by Determining the Accessibility of Thiol Groups. All thiol groups of denatured Ec or Vib IPMDHs (12 or 4 mol/mol of enzyme, respectively) are freely available and react within ~5−10 s with a high concentration (1.3 mM) of Nbs_2. The total number of thiols was found to be 8−10 and 3−3.5 mol/mol for Ec and Vib IPMDHs, respectively, using a molar absorption coefficient (ϵ_{412}) of 14 150 M^{-1} cm^{-1} (*50*). Under native conditions, the Ec enzyme possesses only 2 mol/mol of reactive thiols, while Vib IPMDH has no freely accessible thiols; the buried thiols in both cases react very slowly (over hours). To follow the rates of protein unfolding, aliquots were withdrawn from the denaturation mixture at various times and the number of liberated thiol groups was determined by addition of 1.3 mM Nbs_2. This concentration of Nbs_2 ensures a fast reaction of the free thiols compared to the rate of denaturation. The amount of accessible thiols increases proportionally with the extent of denaturation.

Detection of Refolding by ANS Fluorescence. The concentration of ANS was determined using an extinction coefficient of 4954 M^{-1} cm^{-1} (*51*) at 350 nm in water. Refolding was initiated as described above, except that ANS was present in the renaturation mixture in a 200-fold molar excess over IPMDH. The excitation wavelength was 350 nm, and refolding kinetics were followed at 480 nm. The slits for both excitation and emission were 4 nm.

Structural Analysis Using Molecular Graphics. A data set containing IPMDHs was taken from the Swissprot database, by using the code EC 1.1.1.85 for searching. This search yielded 272 IPMDH sequences, 233 of which were from bacteria and 39 from eukaryotes and archaea.

All 272 sequences were aligned with CLUSTALW. On the basis of this alignment and using a requirement of 95% identity, 46 conserved residues have been identified.

To study the structural origin of thermostability, all sequences were divided into three groups. Eight thermophilic (the few hyperthermophilic, moderate thermophilic, and redundant thermophilic sequences were not considered), 243 mesophilic, and seven psychrophilic IPMDH sequences were found. The single sequence of the psychrotrophic Vib IPMDH was added to the group of psychrophilic IPMDHs. To ensure that there were a comparable number of sequences in each group, only those mesophilic IPMDH sequences that either have an available crystal structure or had been used in earlier mutagenesis studies were kept (altogether eight). We found that these eight mesophilic sequences are adequately representative of the whole mesophilic data set. From the comparison of the three sets of aligned sequences (i.e., eight thermophilic, mesophilic, and psychrophilic IPMDHs each), we selected 27 nonconserved residues that were otherwise closely similar within each group. This selection was based on the following criteria: p*K*, polarity, hydrophobicity, size, and shape (e.g., aliphatic or aromatic) of the amino acid residues. We also examined some other nonconserved residues that were mutated in previous mutagenesis studies with a resulting increase in thermostability.

The molecular contacts of these sets of conserved and nonconserved residues were analyzed via molecular graphics using the crystal structures of Tt [PDB entries 1XAA (*52*) and 1HEX (*43*)] and Ec [PDB entry 1CM7 (*44*)] IPMDHs. In addition, the three-dimensional homology model of Vib IPMDH (*10*), kindly provided by the authors, was used for a similar analysis. For visualizing and analyzing the residue contacts, INSIGHT II (Byosim/MSI, San Diego, CA) was used. The distance limits for hydrogen bonds, hydrophobic interactions, and ionic interactions were 3.5, 4.5, and 4.0 Å, respectively.

Calculation of Contact Order. Both relative and absolute contact order values were calculated on the basis of the formulas given by refs *21* and *53*, respectively, for all nine IPMDHs with known three-dimensional structures [the hyperthermophilic *Sulfolobus tokodaii* (PDB entry 1WPW) and *Thermotoga maritima* (PDB entry 1VLC), the thermophilic Tt (PDB entries 1XAA and 1HEX), the mesophilic Ec (PDB entry 1CM7), *S. typhimurium* (PDB entry 1CNZ), Tf (PDB entry 1A05), *Bacillus coagulans* (PDB entry 2AYQ), and *Mycobacterium tuberculosis* (PDB entry 1W0D)

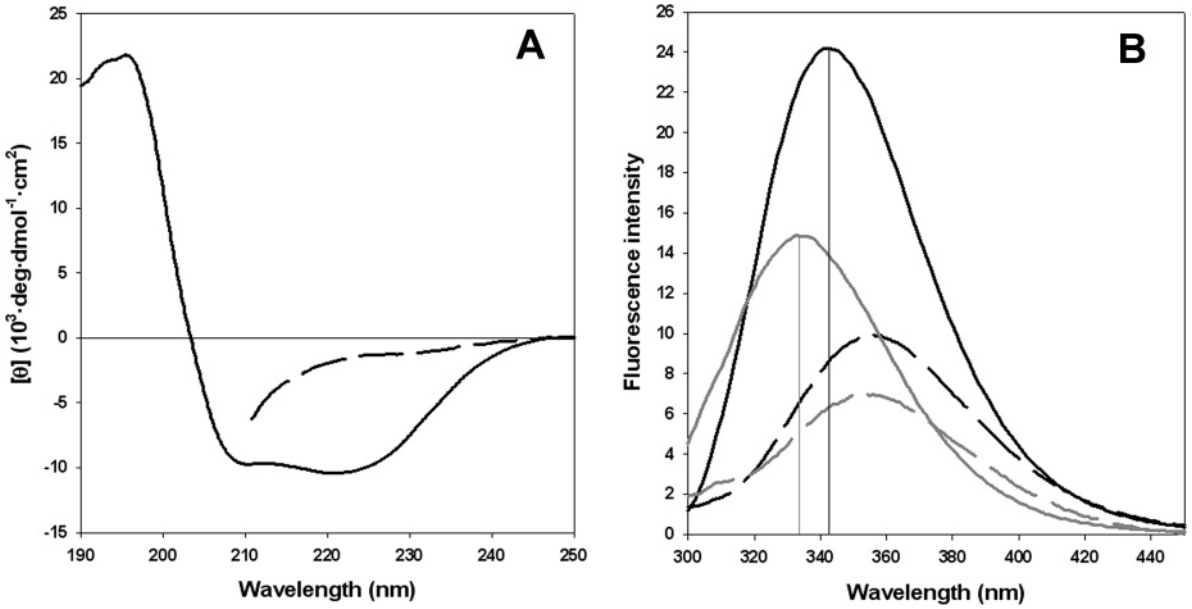

FIGURE 2: Spectral changes accompanying the denaturation of IPMDH. The spectra of native and denatured IPMDHs (shown with solid and dashed lines, respectively) were recorded by both far-UV CD (A) and protein fluorescence emission (B). In panel B, the spectra of Tt and Ec IPMDHs are colored black and gray, respectively. Protein concentrations of 1 mg/mL (16 μM) and 12 μg/mL (0.16 μM) were used in CD (A) and fluorescence (B) measurements, respectively. CD spectra of Ec and Vib IPMDHs (not shown) are similar to that of the Tt enzyme (A). The fluorescence spectrum of Vib IPMDH (not shown) is similar to that of the Ec enzyme (B).

as well as the psychrothropic Vib IPMDHs]. Atomic contacts up to a 6 Å cutoff distance were taken into account.

RESULTS AND DISCUSSION

Spectral Characteristics of Native and Denatured IPMDHs. The change in the far-UV CD spectrum of Tt IPMDH upon the transition from the native to urea-denatured state (*43*) is illustrated in Figure 2A. The CD spectra of native Ec and Vib IPMDHs (not shown) are closely similar to that of the Tt enzyme, as expected from their highly conserved three-dimensional structures (e.g., refs *44*−*46*). The CD spectra of samples equilibrated in 8.5 M urea, however, are characteristic of the completely unfolded states for all IPMDHs.

In contrast, protein fluorescence emission spectra (Figure 2B) exhibit some differences between Tt and Ec IPMDHs, due to the different Trp content of these enzymes. The spectrum of Vib IPMDH (not shown) is indistinguishable from that of Ec IPMDH. Ec and Vib IPMDHs contain two Trp residues per subunit, while Tt IPMDH has an additional Trp in the armlike region. Accordingly, fluorescence emission of Tt IPMDH has a greater intensity, and its λ_{max} is shifted toward higher wavelengths (from 335 to 350 nm) in the native state, compared to that of either Ec or Vib IPMDH. Unfolding is accompanied by a large decrease in the emitted fluorescence intensity and a red shift in λ_{max} (Figure 2B).

Different Rates of Simple First-Order Unfolding of IPMDHs. When the native IPMDHs were manually mixed with urea-containing buffer (dead time of 2−5 s), the unfolding process immediately started and followed a simple first-order time dependence. The observed rate was found to be independent of the technique used for detection [CD, protein fluorescence, thiol reactivity, and enzyme activity (Figure 3A−D, respectively)]. Testing the liberation rate of unreactive (buried) thiol groups upon denaturation (see panel C in Figure 3) was conducted for only Ec and Vib IPMDHs because Tt IPMDH does not contain cysteine.

Comparing the three IPMDHs, we observe that the rate of unfolding increases with a decrease in heat stability (*36*), i.e., in the following order: Tt < Ec < Vib. The experimentally determined first-order rate constants of unfolding for the three IPMDHs are summarized in Table 1. The half-times are ~1 h, several minutes, and a few seconds for the thermophilic, mesophilic, and psychrotrophic variants, respectively. It is also notable that all four monitoring techniques give approximately the same unfolding rate constants, indicating that various regions of the protein molecule and all levels of the structure unfold simultaneously.

When IPMDHs were denatured in the forms of a functioning ternary complex with NAD and Mn*IPM, a nonfunctioning ternary complex with NADH and Mn*IPM, or a binary complex with Mn*IPM, the unfolding was found to be similarly slower than that of the corresponding uncomplexed species. The substrates NAD and NADH, however, separately did not affect the unfolding rates. Thus, bound Mn*IPM alone is responsible for the reduction in the rate of unfolding, probably via stabilization of the enzyme conformation. The crystal structure of Tf IPMDH [PDB entry 1A05 (*45*)] shows that of the 11 conserved residues interacting with bound Mn*IPM, as many as eight are located in separate secondary structure elements (namely, α-helices d, g, and h and β-strands F and G; cf. Figures 1A and 4A). Bound Mn*IPM appears to hold these structural elements together. In addition, it appears that several side chains participating in substrate binding have a stabilizing effect in their own right. These residues are listed in Table 1, and the most interesting interactions are illustrated in panels B−D of Figure 4 in the crystal structure of Tt IPMDH. It may be noted that IPM without the metal ion also provides protection against urea denaturation (data not shown), but to a much smaller extent than Mn*IPM because the interaction of the metal ion with α-helices h and g′ is missing.

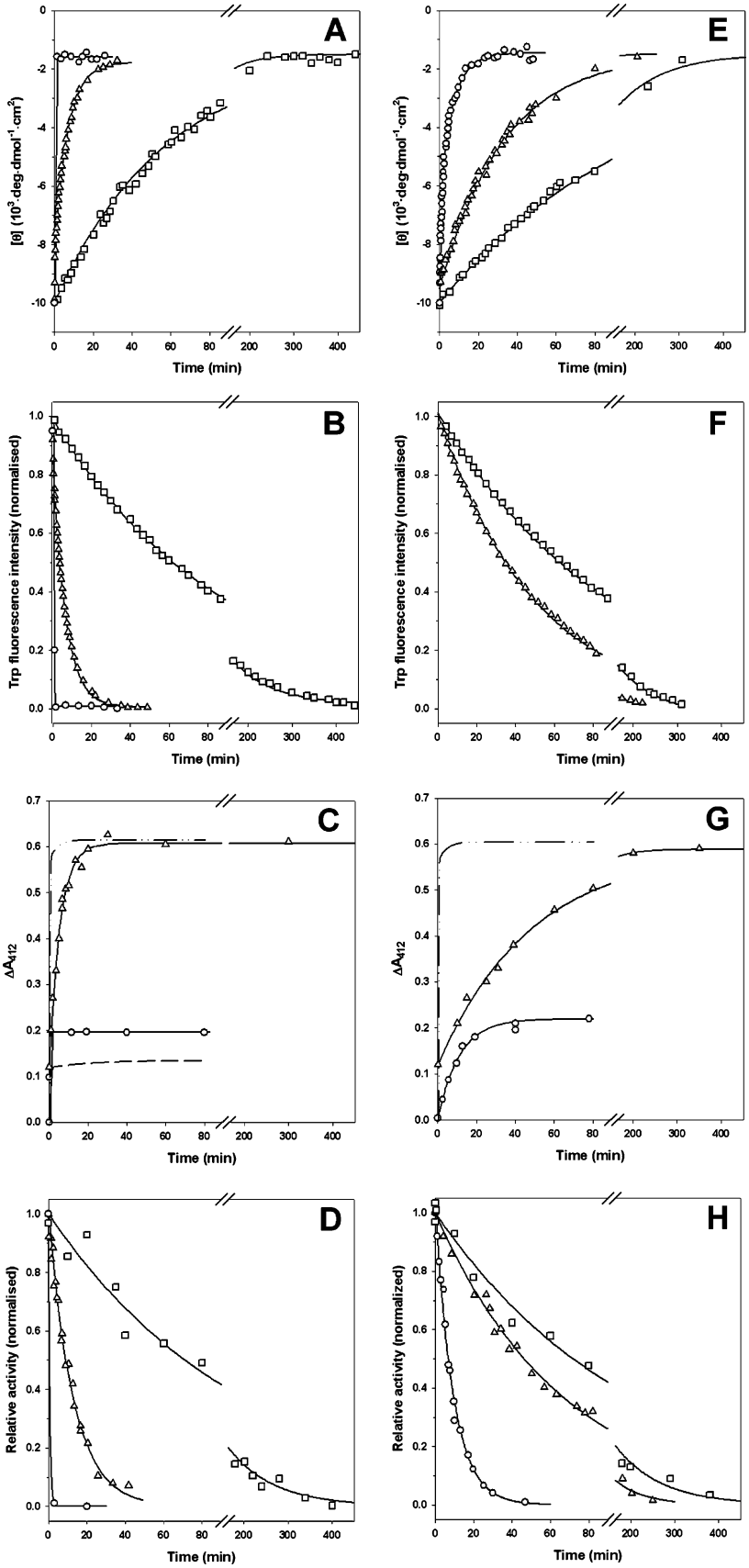

FIGURE 3: Comparison of denaturation time courses of the IPMDHs. Unfolding kinetics curves of Tt (□), Ec (△), and Vib (○) IPMDHs were determined both in the absence of substrates (A−D) and in the presence of Mn*IPM (E−H) by recording the changes in CD (A and E), protein fluorescence spectra (B and F), thiol accessibility (C and G), and enzyme activity (D and H). The protein concentrations were 0.1 mg/mL (1.6 μM) (A and E), 0.01 mg/mL (0.16 μM) (B and F), 0.44 mg/mL (5.9 μM) (C and G), and 0.7 mg/mL (11 μM) (D and H). The solid lines represent curve fitting to a single exponential. The first-order rate constants are summarized in Table 2. In panels C and G, the dash−dot−dot lines represent the time course of thiol modification of the denatured Ec IPMDH with Nbs_2. Under native conditions, the modification of the fast-reacting thiols of Ec IPMDH is plotted with dashed lines.

Table 1: Role of Conserved Side Chains in Substrate Binding and in the Formation of the Tertiary and Quaternary Structures of IPMDHs[a]

Structural part		Selected conserved residues of IPMDHs			Connected secondary structural elements (in parentheses: the contacting residues numbered as in Tt; in Ec and Vib similar interactions exist with the equivalent residues)
		Tt	Ec	Vib	
Domain 1	D	9	13	11	
	G	12	16	14	**βB**(D9)↔**βC**(G73)↔**NAD-loop**(S275)
	E	14	18	16	
	G	*73*	*77*	*75*	**NAD-loop**(281:N,283:N)↔**αa**(E14)
	S	*275*	*286*	*283*	
Inter-domain region	**R**	**94**	**99**	**96**	
	N	102	107	104	
	R	**104**	**109**	**106**	**βE**(S259)↔(N102)**βF**(R104)↔**αh**(D245)
	D	245	255	252	
	S	259	269	266	**αi**(S293)↔**βD**(E270)↔**αd**(R94)
	E	270	281	278	
	S	293	304	301	
Domain 2	**R**	**132**	**138**	**134**	
	E	133	139	135	
	Y	**139**	**145**	**141**	**αh**(D241)↔(R132)**βG**(E133)↔**βL**(Y157)↔**αf**(W195)
	Y	157	167	164	
	R	176	186	183	**αh**(D241)↔**IPM-loop**(Y139)↔**αh**(N237)
	K	**185**	**195**	**192**	
	W	195	205	202	**αe**(R176)↔**βH**(231:O)
	N	237	247	244	
	F	239	249	246	**αh**(F239)↔**βI**(K185)
	D	**241**	**251**	**248**	
	D	245	255	252	
Subunit interface	**K**	**185**	**195**	**192**	**αh'**(D241')↔**αg**(D217)↔**βI**(K185)↔**αf**(V188)
	V	**188**	**198**	**195**	
	D	**217**	**227**	**224**	**αh'**(D241')↔**IPM-loop**(Y139')↔**βI**(K185)
	M	221	231	228	
	Y	**139'**	**145'**	**141'**	**IPM-loop**(Y139')↔**αf**(V188)
	D	**241'**	**251'**	**248'**	
	D	245'	255'	252'	**αh'**(D245')↔**αg**(M221)

[a] Of the 46 identified conserved residues (cf. Materials and Methods and Figure 1B), only those 25 whose importance in maintaining the tertiary fold through side chain contacts could be visualized are listed. Among them are residues that also directly interact with either Mn*IPM (bold) or NAD (italic). The binding details of IPM and the relative positions of the connected secondary structure elements and the atomic details of side chain interactions are illustrated in Figure 4 using the crystal structures of Tt and Tf IMPDHs. A prime denotes a residue from the other subunit.

The extent of the deceleration of unfolding by the bound substrate is markedly different for the three investigated IPMDHs (compare the pairs of panels of Figure 3, A and E, B and F, C and G, and D and H). The corresponding rate constants are listed in Table 2. The deceleration of unfolding by the bound substrate is almost negligible for the most stable thermophilic enzyme, larger for the mesophilic variant, and very large for the psychrotrophic form. This effect is reasonably correlated with the flexibilities of Tt, Ec, and Vib IPMDHs increasing in the same order (*32*, *36*). As a consequence of the different effects of the bound substrate on the unfolding rates, the differences between the unfolding rates of the complexed IPMDHs are smaller than those for the uncomplexed enzymes, but still observable. Taken together, the unfolding rates of IPMDHs strongly and inversely correlate with their different heat stabilities.

Similar Time Courses of the Two-Step or Multistep Refolding of IPMDHs. Refolding of denatured Tt, Ec, and Vib IPMDHs, with a decrease in the urea concentration, was followed by various methods. Monitoring the time course by far-UV CD was not possible because the spectra, reflecting the formation of ~90% of native secondary structure elements, are reconstructed within the dead time of manual mixing (data not shown). This is indicative of the presence of at least one folding intermediate. When refolding kinetics was recorded by measuring the change in the fluorescence intensity of the protein-bound hydrophobic probe ANS (Figure 5A), again an immediate increase within the mixing time was observed (ANS in the presence of either the native or denatured IPMDH has negligible fluorescence). This increase is generally characteristic of the formation of a molten globule state, i.e., an intermediate possessing relatively loosely packed globular structure with the majority of secondary structure elements formed, but without the rigid tertiary structure (*54*, *55*). The immediate increase in ANS fluorescence intensity is followed by a slower decrease reflecting the formation of the protein native structure having a low affinity for ANS. Figure 5A shows only the slow phase of refolding. This slower phase, however, cannot represent a single step because the time course of ANS desorption could not be fitted satisfactorily by assuming a single first-order reaction. It had to be decomposed into at least two sequential first-order steps for proper fitting. This finding reflects the complex nature of the refolding process with more than one intermediate. The results are similar for all three IPMDHs, and the rate constants are listed in Table 3. It is remarkable that ANS desorption occurs on very similar time scales in all three cases, with overall half-times of a few minutes.

The complex nature of IPMDH refolding is also supported by the time course of protein fluorescence (Figure 5B). A burst increase in Trp fluorescence (similar in extent for the three enzymes) is followed by a much slower further increase. The burst change is accompanied by an immediate

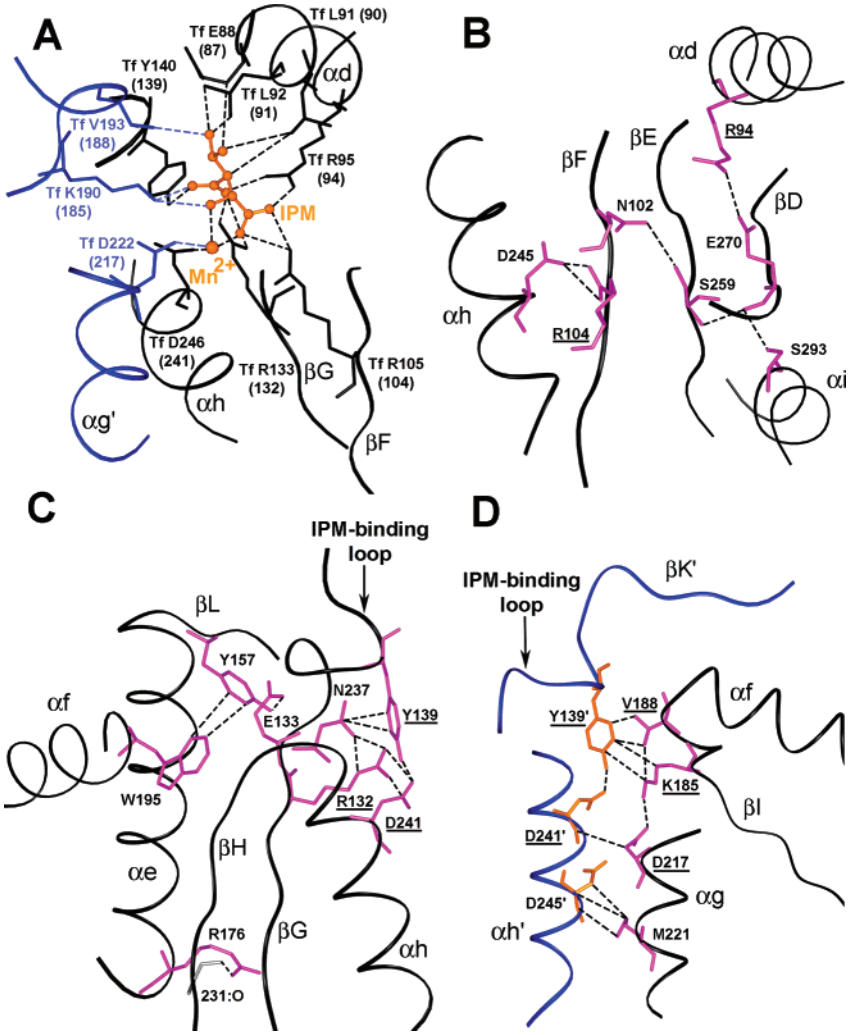

FIGURE 4: Specific interactions among the conserved residues and their interactions with Mn*IPM. The interactions are illustrated both within a single subunit (B and C) and between the two subunits (A and D) using the structural data of Tt IPMDH. The bound Mn*IPM molecule is represented by an orange ball-and-stick model (A). Representative parts of the two subunits, black (A−D) and blue (A and D), are shown with ribbon diagrams. The conserved side chains involved in Mn*IPM binding (A), in the interdomain region (B), in domain 2 (C), and on the subunit interface (D) are represented by black (A), purple (B−D), and orange (D) stick models. The backbones of some nonconserved residues that interact with conserved side chains are colored gray. Dashed lines represent atomic interactions. The residues participating in Mn*IPM binding are underlined in panels B−D.

Table 2: Unfolding Rate Constants (min^{-1}) of the IPMDHs[a]

enzyme	Mn*IPM	far-UV CD	protein fluorescence	activity	thiol reactivity[b]
T. thermophilus	−	0.015 ± 0.003	0.013 ± 0.002	0.010 ± 0.003	−
	+	0.013 ± 0.002	0.012 ± 0.002	0.009 ± 0.002	
E. coli	−	0.14 ± 0.05	0.14 ± 0.06	0.077 ± 0.026	0.14 ± 0.06
	+	0.023 ± 0.004	0.021 ± 0.003	0.015 ± 0.003	0.017 ± 0.003
Vibrio sp. I5	−	>10	>10	>10	>10
	+	0.12 ± 0.04	nd[c]	0.10 ± 0.03	0.087 ± 0.033

[a] The data were obtained by fitting the experimental results of Figure 3 to a single first-order process. [b] Tt IPMDH has no thiol groups. [c] Not determined.

shift in λ_{max} from the value characteristic of the denatured state to that of the native state (data not shown). Thus, during the burst phase, an intermediate is formed which may correspond to the molten globule-like intermediate. In the slower phase of the kinetics (measurable on a time scale of several minutes), the extent of the fluorescence increase is much larger for Tt IPMDH than those observed for the Ec and Vib enzymes, the latter two being similar to each other. It is reasonable to assume that the larger change in fluorescence intensity for Tt IPMDH during the slower step is due to the additional Trp residue located in the armlike region of the subunit, which is missing in both Ec and Vib IPMDHs. The differences in the rate constants of the slow parts of the fluorescence changes (Table 3) may be partly due to the same reason.

We could assume that the larger increase in protein fluorescence for Tt IPMDH during the slow phase may reflect the formation of nativelike subunit−subunit contacts between the two arms. If this assumption is correct, the slow process could be identified as a bimolecular association step of the two polypeptide chains. To test this assumption, we repeated the refolding experiments monitored by protein

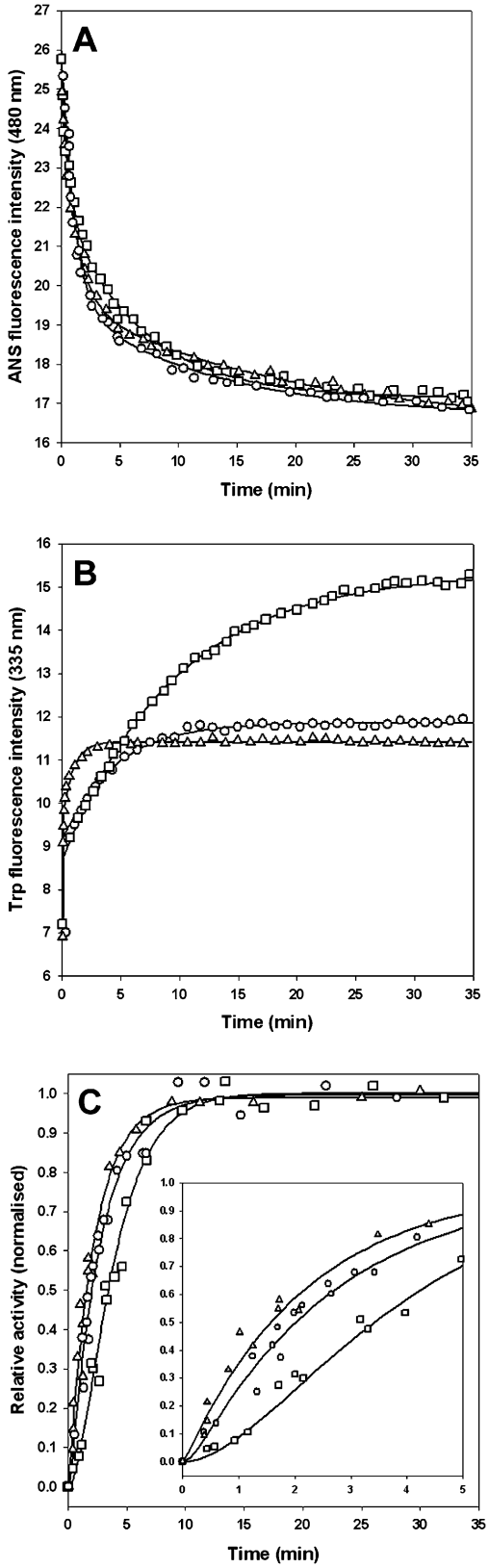

FIGURE 5: Comparison of renaturation time courses of the IPMDHs. Refolding kinetic curves of Tt (□), Ec (△), and Vib (○) IPMDHs were determined by recording the changes of the bound ANS fluorescence (A), protein fluorescence (B), and enzyme activity (C). The protein concentrations were 6 μg/mL (0.08 μM) (A and C) and 12 μg/mL (0.16 μM) (B). In the inset of panel C, the initial parts of the time courses are enlarged. The time courses shown in panels A−C are fitted to the equation of a two-step first-order sequential mechanism. The corresponding rate constants are given in Table 3.

fluorescence at various enzyme concentrations (from 0.04 to 1.60 μM) for all three enzymes but found no dependence of the time courses on enzyme concentration (data not shown). The kinetic analysis uniformly yielded rate constants similar to those listed in Table 3. Thus, the assumption about dimer formation as a rate-limiting step during the slow phase is not supported. The occurrence of dimer formation during this step, however, cannot be excluded; its rate could be limited by a preceding, even slower intramolecular isomerization step.

Measurements of reactivation during refolding provided further evidence of the existence of an intermediate state. The time courses of reactivation exhibit an interesting feature: a small but real lag phase was observed with all three IPMDHs. This lag phase is most pronounced in the case of the Tt enzyme (Figure 5C). This indicates that restoration of the enzymatically active structure during refolding is a complex process and occurs through the formation of an intermediate with small or no activity. The time courses do not depend on the concentration of protein in the renaturation mixture. Thus, like the fluorescence results, no evidence of the involvement of a bimolecular association step in the reactivation process or the presence of a monomeric, inactive intermediate was obtained. The reactivation time courses can be described by a kinetic model including two sequential first-order steps with an inactive intermediate (see the inset in Figure 5C). The rate constants of the entire process are summarized in Table 3. Apart from the complex nature of the reactivation process, it should be noted that it occurs on comparable time scales (with overall half-times of 2−3 min) for all three IPMDHs.

Nature of IPMDH Folding Intermediate(s). As mentioned in the introductory section, the formation of a dimeric intermediate during the unfolding of IPMDH was suggested in earlier studies (*30*, *33*), but the kinetics of unfolding and refolding have not been investigated. The kinetic studies of refolding presented here clearly show the existence of inactive intermediate species of all three IPMDHs, but no bimolecular (second-order) dimerization step could be identified (at least during the slow phase of refolding). It is possible that this intermediate is already an associated form of the two polypeptide chains, and therefore, association is not a rate-limiting step during the slower part of refolding. Alternatively, the rate of dimer formation may be limited by a preceding slow isomerization step. To determine the nature of the intermediate, further work is required, but this is beyond the scope of this comparative study.

Interpretation of the Similar Refolding and Different Unfolding Rates in Light of the Structural Features of IPMDHs. Our results do not show a correlation between folding rate and stability for IPMDHs. Most studies in the literature investigating the determinants of folding rates are about single-domain proteins with two-state folding kinetics. These studies demonstrated an inverse relationship between the folding rate and the complexity of the native topology, characterized by the contact order, CO (the average residue separation of atomic contacts) (*21*, *25*, *26*, *56*−*58*). For proteins with three-state folding kinetics, an inverse correlation was observed with protein length (*59*). The chain length was taken into account by the recent definition of absolute CO, which shows a clear inverse relationship with the folding rate of single-domain proteins having two-state or multistate

Table 3: Refolding Rate Constants (min^{-1}) of the IPMDHs[a]

	protein fluorescence		ANS desorption		activity	
enzyme	k_1	k_2	k_1	k_2	k_1	k_2
T. thermophilus	>20	0.11 ± 0.02	0.67 ± 0.13	0.12 ± 0.01	0.96 ± 0.20	0.26 ± 0.05
E. coli	>20	0.80 ± 0.20	0.76 ± 0.10	0.064 ± 0.006	>20	0.46 ± 0.07
Vibrio sp. I5	>20	0.23 ± 0.03	0.77 ± 0.10	0.064 ± 0.003	7.2 ± 1.2	0.37 ± 0.05

[a] The data were obtained by fitting the experimental results of Figure 5 to the equations describing two first-order sequential steps, characterized by rate constants k_1 and k_2. For reactivation, an intermediate species with no activity was assumed for the rate equation, like in Szilágyi and Vas (*72*). In some cases, the rate constant for the fast phase (k_1) must be treated with caution because of the large experimental error.

folding kinetics (*53*). Furthermore, a higher CO (implying a lower folding rate) was found for most of the hyperthermophilic bacterium *T. maritima* proteins compared to their mesophilic counterparts (*28*). On this basis, for IPMDHs with different heat stabilities, different folding rates could have been expected: the most stable variant should have the lowest folding rate. On the contrary, similar refolding rates were found. To test the relationship between the folding rates of IPMDHs and CO or chain length, we calculated both relative and absolute contact orders for all nine available IPMDH structures (cf. Materials and Methods). No relationship is observed between thermostability and either contact order or chain length, since both values are found to be very similar among IPMDHs with different heat stabilities. Namely, the average values of the relative as well as the absolute contact order are 0.07776, 0.07826, and 0.07564 as well as 26.80, 27.75, and 27.23 for the thermophilic, mesophilic, and psychrotrophic variants, respectively. However, the chain length of the presently studied Tt IPMDH is somewhat shorter (345 residues) than the average lengths of any of the three groups of IPMDHs (i.e., 358, 360, and 361), but this would imply faster folding, which contradicts the results presented here. Thus, the experimental data for the three IPMDHs do not follow the tendency observed with other proteins (*28*, *59*). The present data, however, are in accordance with the similar contact orders, especially the absolute CO, for the proteins exhibiting similar folding rates. In summary, our data and other studies (*24*, *60*) demonstrate that the relationship among contact order, stability, and folding rate is not clear-cut and varies between proteins. To reach more general conclusions, additional data for other multidomain and multisubunit proteins, preferably adapted to various temperatures, are needed.

As for unfolding, the different rates observed with the three investigated IPMDHs are in agreement with the data obtained with some other proteins where slower unfolding was found for proteins with higher thermostability (*12*−*14*, *17*). Here we have attempted to relate the unfolding rates to specific structural properties of IPMDHs with different heat stabilities. We compared the atomic contacts made by the selected nonconserved residues in Tt, Ec, and Vib IPMDHs. Of the 27 investigated nonconserved residues, as many as 16 were found where the observed differences in the atomic contacts are clearly in line with the different thermostabilities. These residues are listed in Table 4. The importance of nonconserved residues in adjusting protein stability is also supported by mutational studies (*34*, *38*, *52*, *61*−*65*).

This analysis has identified three particular regions of the IPMDH molecule that may have the greatest influence on thermostability. The first region is within domain 1 and holds together secondary elements αa, αi, αj, and αk (Figure 6A), as well as αa and βA (Figure 6C). These interactions include the N- and C-termini of the polypeptide chain, i.e., the region of domain 1 where stabilization by conserved side chains appears to be less prominent. The importance of contacts between N- and C-terminal residues is also demonstrated by mutagenesis studies (*66*, *67*). Besides the long-range stabilization effects, short-range effects have also been identified, such as the stabilization of the loop preceding αc (Figure 6D). Within domain 2, very few stabilizing interactions involving nonconserved residues have been found (e.g., Figure 6E).

The second important part is the interdomain region. One example is residue Tt L115, Ec F120, or Vib A117, which strengthens the interaction between the three flexible loops (namely, βF−βG, αh−βE, and αj−αk) located between the two domains (Figure 6B). The stabilizing role of a hydrophobic residue at this position has also been shown by a mutagenesis study (*63*). The essential role of the βF−βG loop in the increased thermostability and possibly in the unfolding process is supported by a temperature jump experiment as detected by fast crystallographic methods (*35*). Presumably, the initial structural change at the start of unfolding occurs in this region. The molecular contacts, differing between the three IPMDHs as depicted in Figure 6B, are clearly in accordance with the different stabilities.

The third stabilizing region includes the subunit−subunit interface. Several previous mutational studies (*34*, *41*, *68*−*70*) suggested that the interactions within the two interacting arms (including βK and βL) and their interactions with αf, as well as the four-helix bundle (consisting of helices g, g′, h, and h′), are much more favorable in the thermophilic variant than in the mesophilic form. Our structural analysis shows that all the previously observed relationships between structure and stability, and those suggested here, can be extended to the psychrophilic forms as well.

Taking the unfolding−refolding kinetic results into account, we may also hypothesize that the molecular differences characteristic of the native folded states are not yet reflected by the transition states. This follows from the fact that while the transition states of the unfolding reactions are located at different heights with respect to the energetic positions of their native states, the transition states for the folding reactions are at the same energy level relative to the denatured states. Thus, the transition states on the main free energy barrier separating the native and denatured states of the three proteins may be structurally similar to each other. Early intermediates on the protein refolding pathway are also similar in these respects. Thus, the structural differences in the folded states of different IPMDHs are not conserved in the transition and intermediate states. The transition state probably represents an early phase of the refolding reaction

Table 4: Role of Nonconserved Side Chains in the Different Structural Stabilities of IPMDHs[a]

structure part	selected nonconserved residues in IPMDH groups of different thermal stabilities: thermophiles		mesophiles		psychrophiles		change in the nature of side chains with a decrease in thermostability	ref	structural basis of different thermostabilities and the elements involved (from comparison of Tt, Ec, and Vib structures)
	Tt		Ec		Vib[b]				
domain 1	E17	(1A, 1S, 1Q, 2E, 3R)	T21	(3A, 1T, 1D, 2E)	A19	(3A, 1V, 1L, 2T, 1E)	charged → hydrophobic	*73*	stabilization in Tt within αa and connection of **αa** with ***β*A** (Figure 6C)
	R24	(1Q, 2D, 2R, 3K)	D28	(1T, 3D, 4K)	N26	(1V, 5N, 2D)	charged → polar		
	Y36	(1I, 3F, 2Y, 2W)	T40	(2T, 1C, 5F)	L38	(3L, 1M, 1F, 1T, 2R)	decrease in side chain volume	*74*	
	L26	(1A, 4V, 2L, 1I)	V30	(1A, 6V, 1I)	A28	(1A, 6V, 1L)	decrease in chain length	*66*, *67*	stabilization in Tt and Ec by connecting αa simultaneously with **αi**, **αj**, and **αk** (Figure 6A)
	V311	(4V, 4I)	I322	(4V, 4I)	I319	(8I)	increase in chain length	–	
	E321	(4Q, 4E)	E332	(1A, 2S, 1Q, 1D, 3E)	Q329	(2A, 1N, 2Q, 2D, 1R)	decreasing probability of ionic interactions	*73*	stabilization by ionic (Tt) and H-bonding (Ec) interactions between **αj** and **αk** (Figure 6A)
	H343	(1A, 1L, 2H, 1E, 3K)	Y358	(2A, 1I, 1F, 2Y, 1K, 1R)	A356	(3A, 1Y, 1Q, 1R, 2K)			
	F53	(4L, 3F, 1Y)	L57	(8L)	L55	(8L)	decrease in side chain volume	*65*	stabilization in Tt between **αc** and the preceding loop (Figure 6B)
	R58	(4L, 4R)	V62	(3V, 4L, 1I)	L60	(1V, 5L, 2M)	decrease in basicity		
	R82	(1G, 2P, 1W, 4R)	P86	(1G, 1A, 1S, 4P, 1del)	P84	(5P, 3R)	charged → hydrophobic	*52*, *61*, *63*	stabilization through surface charges (only in the chimeric enzyme 2T2M6T)
	A290	(4A, 1M, 1T, 2Q)	Q301	(1A, 3T, 4Q)	T298	(4T, 3Q, 1E)	increase in polarity	–	polarity within the hydrophobic core would decrease the stability in the connection between αa and αi
domain 2	P110	(7P, 1D)	Q115	(1A, 2P, 1S, 1E, 2Q, 1N)	P112	(5P, 1S, 1E, 1K)	*c*	*35*, *63*, *70*, *75*	Pro-Gly motive at the end of ***β*F** increases the rigidity and thereby increases the stability of Tt
	G111	(2G, 2S, 1P, 3Q)	G116	(2G, 1V, 1S, 1T, 2E, 1Q)	Q113	(1G, 2A, 1S, 4Q)			
	E113	(3V, 1L, 2K, 2E)	E118	(3L, 1S, 2E, 2K)	A115	(1A, 3V, 2S, 1T, 1E)			
	L115	(6A, 2L)	F120	(5A, 1D, 2F)	A117	(6A, 1L, 1F)	*c*	*63*	interdomain loops between ***β*F** and ***β*G**, **αh** and ***β*E**, and **αk** and **αj** are connected only in Tt
	R177	(1Q, 6R, 1K)	R187	(2N, 5R, 1K)	G184	(1G, 2A, 3S, 1N, 1E)	decrease in basicity	–	connection of ***β*G** with the loop between **αe** and ***β*I** in Tt, weak in Ec, and not in Vib (Figure 6)
interdomain region	V126	(5V, 1L, 2I)	F132	(4V, 1L, 2F, 1T)	L128	(4L, 4F)	increase in side chain volume	*38*, *62*, *64*	increase in side chain volume causes overcrowding at the hydrophobic interdomain region in Ec and Vib
	A172	(3A, 3L, 1I, 1T)	S182	(3A, 1L, 2M, 2S)	M179	(4A, 2L, 1M, 1S)	*c*	*31*, *76*, *77*	increase in van der Waals volume would improve the stability by strengthening the hydrophobic domain−domain interaction between **αe** and **αi**
	H300	(1L, 3H, 4Y)	Y311	(1L, 1T, 5Y, 1H)	Y308	(1F, 7Y)	*c*	*78*	
subunit interface	M146	(4I, 2M, 1R, 1K)	R152	(1L, 1T, 1D, 5R)	K149	(7R, 1K)	increase in basicity	–	charged residues at the intersubunit surface (including **αf**, ***β*K**, and ***β*L)** in Ec and Vib weaken hydrophobic interactions
	N153	(6N, 2D)	D163	(1N, 7D)	D160	(2N, 6D)	increase in acidity	–	
	E190	(1S, 7E)	Q200	(1A, 1T, 2Q, 1D, 3E)	A197	(3A, 1T, 1Q, 3E)	decrease in acidity	*34*	salt bridge connection between **αf** and ***β*K′** in Tt, but not in Ec and Vib (in Vib, another salt bridge exists, but between ***β*K** and ***β*L**)
	F194	(6L, 2F)	L204	(6L, 1M, 1F)	L201	(7L, 1F)	*c*	*69*	hydrophobic interaction of αf with ***β*K′** and ***β*L′** is strengthened in Tt, but not in Ec and Vib
	L246	(2L, 1I, 5E)	E256	(8E)	E253	(1I, 7E)	*c*	*68*, *70*	increase in the van der Waals volume causes overcrowding in Ec and Vib at the hydrophobic four-helix bundle connection
	V249	(2V, 5M, 1Q)	M259	(2V, 1I, 4M, 1Q)	M256	(8M)	*c*	*41*, *68*	

[a] Of the selected 27 nonconserved residues with properties unique to each group of thermophiles, mesophiles, and psychrophiles (cf. Materials and Methods), only those 16 for which a correlation with the different stabilities was found by graphical comparison are listed. Among them are five residues (53, 58, 82, 126, and 190 in Tt numbering), the stabilization roles of which have been confirmed by site-directed mutagenesis studies. There are nine other nonconserved side chains for which experimental evidence (site-directed mutagenesis) suggests a role in thermal stability, but no consistent correlation has been found between thermostability and the chemical nature of the side chain. For each position, the amino acid residues occurring in each eight-member group, i.e., thermophiles, mesophiles, and psychrophiles, are given in parentheses. [b] Vib IPMDH is a psychrotrophic enzyme. [c] No consistent trend is seen, but mutagenesis studies gave positive results.

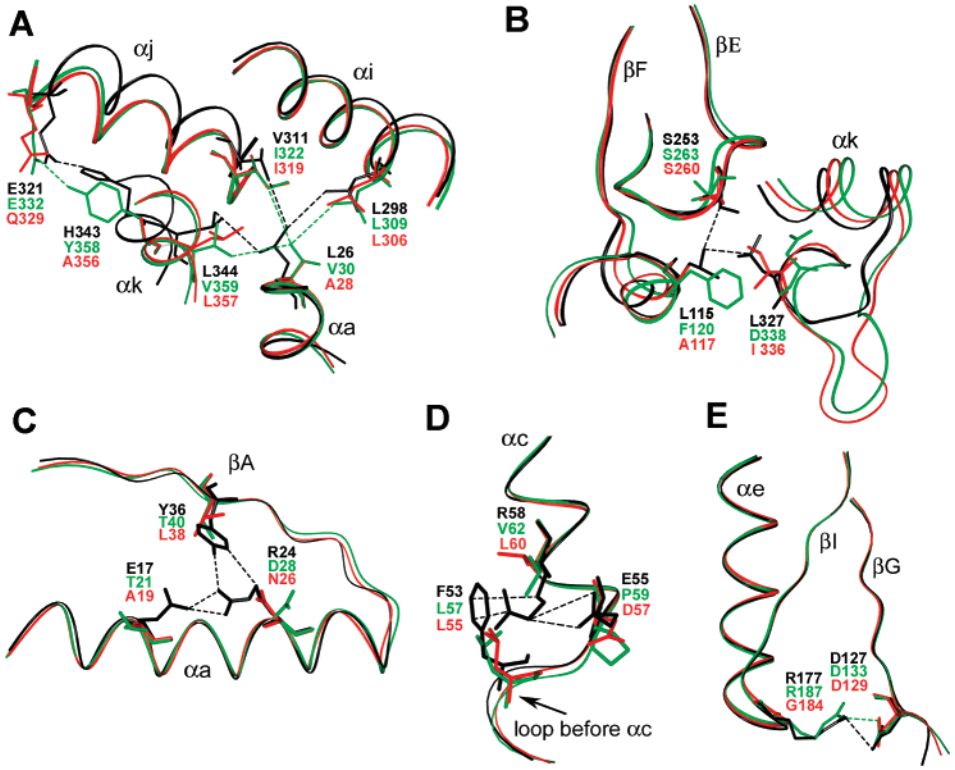

FIGURE 6: Structural differences between IPMDHs with different thermostabilities. The secondary structure elements are represented by black (Tt), green (Ec), and red (Vib) ribbon diagrams. The three structures were superimposed by the Cα atoms of all β-strands except βK and βL. The nonconserved side chains are shown as stick models in the respective colors. Dashed lines (colored as the corresponding structure) represent atomic interactions. Panels A, C, and D show selected details of domain 1; panel B illustrates the interdomain region, and panel E refers to domain 2.

coordinate, where only the main chain topology is formed (as the rate-determining step of the folding process), which is accompanied by a large decrease in the protein chain entropy. The structural differences between the proteins are formed only during the subsequent or final stages of folding by specific packing of the amino acid side chains. Such interpretation is in accordance with the conclusions drawn from a recent theoretical study of a large set of thermophilic and mesophilic proteins (*71*).

In summary, these experimental unfolding−refolding studies and the structural and thermodynamic analysis of the IPMDH variants have shown that their different heat stabilities are not related to their (similar) folding rates but are due to their different unfolding rates. Unfolding rates may be determined by a variety of molecular contacts of the nonconserved residues, especially in the interdomain region and in domain 1, including the contacts between the N- and C-termini. On the other hand, the folding rate appears to be determined by the similar structural and thermodynamic features of the transition and intermediate states, i.e., by more global structural characteristics (such as native topology, i.e., contact order) of the various IPMDHs and not necessarily related to the different thermodynamic stabilities of their native states.

REFERENCES

1. Russell, N. J. (2000) Toward a molecular understanding of cold activity of enzymes from psychrophiles, *Extremophiles 4*, 83−90.
2. Szilágyi, A., and Závodszky, P. (2000) Structural differences between mesophilic, moderately thermophilic and extremely thermophilic protein subunits: Results of a comprehensive survey, *Struct. Folding Des. 8*, 493−504.
3. Sterner, R., and Liebl, W. (2001) Thermophilic adaptation of proteins, *Crit. Rev. Biochem. Mol. Biol. 36*, 39−106.
4. Vieille, C., and Zeikus, G. J. (2001) Hyperthermophilic enzymes: Sources, uses, and molecular mechanisms for thermostability, *Microbiol. Mol. Biol. Rev. 65*, 1−43.
5. Georlette, D., Blaise, V., Collins, T., D'Amico, S., Gratia, E., Hoyoux, A., Marx, J. C., Sonan, G., Feller, G., and Gerday, C. (2004) Some like it cold: Biocatalysis at low temperatures, *FEMS Microbiol. Rev. 28*, 25−42.
6. Yokota, K., Satou, K., and Ohki, S. (2006) Comparative analysis of protein thermo stability: Differences in amino acid content and substitution at the surfaces and in the core regions of thermophilic and mesophilic proteins, *Sci. Technol. Adv. Mater. 7*, 255−262.
7. Razvi, A., and Scholtz, J. M. (2006) Lessons in stability from thermophilic proteins, *Protein Sci. 15*, 1569−1578.
8. Sadeghi, M., Naderi-Manesh, H., Zarrabi, M., and Ranjbar, B. (2006) Effective factors in thermostability of thermophilic proteins, *Biophys. Chem. 119*, 256−270.
9. Magyar, C., Szilágyi, A., and Závodszky, P. (1996) Relationship between thermal stability and 3-D structure in a homology model of 3-isopropylmalate dehydrogenase from *Escherichia coli*, *Protein Eng. 9*, 663−670.
10. Wallon, G., Lovett, S. T., Magyar, C., Svingor, A., Szilágyi, A., Závodszky, P., Ringe, D., and Petsko, G. A. (1997) Sequence and homology model of 3-isopropylmalate dehydrogenase from the psychrotrophic bacterium *Vibrio* sp. I5 suggest reasons for thermal instability, *Protein Eng. 10*, 665−672.
11. Robinson-Rechavi, M., Alibes, A., and Godzik, A. (2006) Contribution of electrostatic interactions, compactness and quaternary structure to protein thermostability: Lessons from structural genomics of *Thermotoga maritime*, *J. Mol. Biol. 356*, 547−557.
12. Cavagnero, S., Debe, D. A., Zhou, Z. H., Adams, M. W., and Chan, S. I. (1998) Kinetic role of electrostatic interactions in the

unfolding of hyperthermophilic and mesophilic rubredoxins, *Biochemistry 37*, 3369−3376.
13. Perl, D., Welker, C., Schindler, T., Schroder, K., Marahiel, M. A., Jaenicke, R., and Schmid, F. X. (1998) Conservation of rapid two-state folding in mesophilic, thermophilic and hyperthermophilic cold shock proteins, *Nat. Struct. Biol. 5*, 229−235.
14. Ogasahara, K., Nakamura, M., Nakura, S., Tsunasawa, S., Kato, I., Yoshimoto, T., and Yutani, K. (1998) The unusually slow unfolding rate causes the high stability of pyrrolidone carboxyl peptidase from a hyperthermophile, *Pyrococcus furiosus*: Equilibrium and kinetic studies of guanidine hydrochloride-induced unfolding and refolding, *Biochemistry 37*, 17537−17544.
15. Cao, A., Wang, G., Tang, Y., and Lai, L. (2002) Linear correlation between thermal stability and folding kinetics of lysozyme, *Biochem. Biophys. Res. Commun. 291*, 795−797.
16. Hollien, J., and Marqusee, S. (2002) Comparison of the folding processes of *T. thermophilus* and *E. coli* ribonucleases H, *J. Mol. Biol. 316*, 327−340.
17. Wittung-Stafshede, P. (2004) Slow unfolding explains high stability of thermostable ferredoxins: Common mechanism governing thermostability, *Biochim. Biophys. Acta 1700*, 1−4.
18. Dams, T., and Jaenicke, R. (1999) Stability and folding of dihydrofolate reductase from the hyperthermophilic bacterium *Thermotoga maritime*, *Biochemistry 38*, 9169−9178.
19. Finkelstein, A. V. (1991) Rate of β-structure formation in polypeptides, *Proteins 9*, 23−27.
20. Shakhnovich, E., Abkevich, V., and Ptitsyn, O. (1996) Conserved residues and the mechanism of protein folding, *Nature 379*, 96−98.
21. Plaxco, K. W., Simons, K. T., and Baker, D. (1998) Contact order, transition state placement and the refolding rates of single domain proteins, *J. Mol. Biol. 277*, 985−994.
22. Fersht, A. R. (2000) Transition-state structure as a unifying basis in protein-folding mechanisms: Contact order, chain topology, stability, and the extended nucleus mechanism, *Proc. Natl. Acad. Sci. U.S.A. 97*, 1525−1529.
23. Dinner, A. R., Sali, A., Smith, L. J., Dobson, C. M., and Karplus, M. (2000) Understanding protein folding via free-energy surfaces from theory and experiment, *Trends Biochem. Sci. 25*, 331−339.
24. Clarke, J., Cota, E., Fowler, S. B., and Hamill, S. J. (1999) Folding studies of immunoglobulin-like β-sandwich proteins suggest that they share a common folding pathway, *Structure 7*, 1145−1153.
25. Plaxco, K. W., Larson, S., Ruczinski, I., Riddle, D. S., Thayer, E. C., Buchwitz, B., Davidson, A. R., and Baker, D. (2000) Evolutionary conservation in protein folding kinetics, *J. Mol. Biol. 298*, 303−312.
26. Dinner, A. R., and Karplus, M. (2001) The roles of stability and contact order in determining protein folding rates, *Nat. Struct. Biol. 8*, 21−22.
27. Kaushik, J. K., Ogasahara, K., and Yutani, K. (2002) The unusually slow relaxation kinetics of the folding-unfolding of pyrrolidone carboxyl peptidase from a hyperthermophile, *Pyrococcus furiosus*, *J. Mol. Biol. 316*, 991−1003.
28. Robinson-Rechavi, M., and Godzik, A. (2005) Structural genomics of *Thermotoga maritima* proteins shows that contact order is a major determinant of protein thermostability, *Structure 13*, 857−860.
29. Wiebe, W. J., Sheldon, W. M., and Pomeroy, L. R. (1992) Bacterial Growth in the Cold: Evidence for an Enhanced Substrate Requirement, *Appl. Environ. Microbiol. 58*, 359−364.
30. Hayashi-Iwasaki, Y., Numata, K., Yamagishi, A., Yutani, K., Sakurai, M., Tanaka, N., and Oshima, T. (1996) A stable intermediate in the thermal unfolding process of a chimeric 3-isopropylmalate dehydrogenase between a thermophilic and a mesophilic enzymes, *Protein Sci. 5*, 511−516.
31. Akanuma, S., Qu, C., Yamagishi, A., Tanaka, N., and Oshima, T. (1997) Effect of polar side chains at position 172 on thermal stability of 3-isopropylmalate dehydrogenase from *Thermus thermophilus*, *FEBS Lett. 410*, 141−144.
32. Závodszky, P., Kardos, J., Svingor, Á., and Petsko, G. A. (1998) Adjustment of conformational flexibility is a key event in the thermal adaptation of proteins, *Proc. Natl. Acad. Sci. U.S.A. 95*, 7406−7411.
33. Motono, C., Yamagishi, A., and Oshima, T. (1999) Urea-induced unfolding and conformational stability of 3-isopropylmalate dehydrogenase from the thermophile *Thermus thermophilus* and its mesophilic counterpart from *Escherichia coli*, *Biochemistry 38*, 1332−1337.
34. Németh, A., Svingor, A., Pocsik, M., Dobó, J., Magyar, C., Szilágyi, A., Gál, P., and Závodszky, P. (2000) Mirror image mutations reveal the significance of an intersubunit ion cluster in the stability of 3-isopropylmalate dehydrogenase, *FEBS Lett. 468*, 48−52.
35. Hori, T., Moriyama, H., Kawaguchi, J., Hayashi-Iwasaki, Y., Oshima, T., and Tanaka, N. (2000) The initial step of the thermal unfolding of 3-isopropylmalate dehydrogenase detected by the temperature-jump Laue method, *Protein Eng. 13*, 527−533.
36. Svingor, A., Kardos, J., Hajdú, I., Németh, A., and Závodszky, P. (2001) A better enzyme to cope with cold. Comparative flexibility studies on psychrotrophic, mesophilic, and thermophilic IPMDHs, *J. Biol. Chem. 276*, 28121−28125.
37. Motono, C., Oshima, T., and Yamagishi, A. (2001) High thermal stability of 3-isopropylmalate dehydrogenase from *Thermus thermophilus* resulting from low $\Delta\Delta C_p$ of unfolding, *Protein Eng. 14*, 961−966.
38. Suzuki, T., Yasugi, M., Arisaka, F., Yamagishi, A., and Oshima, T. (2001) Adaptation of a thermophilic enzyme, 3-isopropylmalate dehydrogenase, to low temperatures, *Protein Eng. 14*, 85−91.
39. Yasugi, M., Suzuki, T., Yamagishi, A., and Oshima, T. (2001) Analysis of the effect of accumulation of amino acid replacements on activity of 3-isopropylmalate dehydrogenase from *Thermus thermophilus*, *Protein Eng. 14*, 601−607.
40. Yasugi, M., Amino, M., Suzuki, T., Oshima, T., and Yamagishi, A. (2001) Cold adaptation of the thermophilic enzyme 3-isopropylmalate dehydrogenase, *J. Biochem. 129*, 477−484.
41. Ohkuri, T., and Yamagishi, A. (2003) Increased thermal stability against irreversible inactivation of 3-isopropylmalate dehydrogenase induced by decreased van der Waals volume at the subunit interface, *Protein Eng. 16*, 615−621.
42. Imada, K., Sato, M., Tanaka, N., Katsube, Y., Matsuura, Y., and Oshima, T. (1991) Three-dimensional structure of a highly thermostable enzyme, 3-isopropylmalate dehydrogenase of *Thermus thermophilus* at 2.2 Å resolution, *J. Mol. Biol. 222*, 725−738.
43. Hurley, J. H., and Dean, A. M. (1994) Structure of 3-isopropylmalate dehydrogenase in complex with NAD^+: Ligand-induced loop closing and mechanism for cofactor specificity, *Structure 2*, 1007−1016.
44. Wallon, G., Kryger, G., Lovett, S. T., Oshima, T., Ringe, D., and Petsko, G. A. (1997) Crystal structures of *Escherichia coli* and *Salmonella typhimurium* 3-isopropylmalate dehydrogenase and comparison with their thermophilic counterpart from *Thermus thermophilus*, *J. Mol. Biol. 266*, 1016−1031.
45. Imada, K., Inagaki, K., Matsunami, H., Kawaguchi, H., Tanaka, H., Tanaka, N., and Namba, K. (1998) Structure of 3-isopropylmalate dehydrogenase in complex with 3-isopropylmalate at 2.0 Å resolution: The role of Glu88 in the unique substrate-recognition mechanism, *Structure 6*, 971−982.
46. Singh, R. K., Kefala, G., Janowski, R., Mueller-Dieckmann, C., von Kries, J. P., and Weiss, M. S. (2005) The high-resolution Structure of LeuB (Rv2995c) from *Mycobacterium tuberculosis*, *J. Mol. Biol. 346*, 1−11.
47. Kagawa, Y., Nojima, H., Nukiwa, N., Ishizuka, M., Nakajima, T., Yasuhara, T., Tanaka, T., and Oshima, T. (1984) High guanine plus cytosine content in the third letter of codons of an extreme thermophile. DNA sequence of the isopropylmalate dehydrogenase of *Thermus thermophilus*, *J. Biol. Chem. 259*, 2956−2960.
48. Yamada, T., Akutsu, N., Miyazaki, K., Kakinuma, K., Yoshida, M., and Oshima, T. (1990) Purification, catalytic properties, and thermal stability of threo-DS-3-isopropylmalate dehydrogenase coded by leuB gene from an extreme thermophile, *Thermus thermophilus* strain HB8, *J. Biochem. 108*, 449−456.
49. Pace, C. N., Vajdos, F., Fee, L., Grimsley, G., and Gray, T. (1995) How to measure and predict the molar absorption coefficient of a protein, *Protein Sci. 4*, 2411−2423.
50. Riddles, P. W., Blakeley, R. L., and Zerner, B. (1979) Ellman's reagent: 5,5′-Dithiobis(2-nitrobenzoic acid)—a reexamination, *Anal. Biochem. 94*, 75−81.
51. Weber, G., and Young, B. (1964) Fragmentation of bovine serum albumin by pepsin. I. The origin of the acid expansion of the albumin molecule, *J. Biol. Chem. 239*, 1415−1423.
52. Nagata, C., Moriyama, H., Tanaka, N., Nakasako, M., Yamamoto, M., Ueki, T., and Oshima, T. (1996) Cryocrystallography of 3-isopropylmalate dehydrogenase from *Thermus thermophilus* and its chimeric enzyme, *Acta Crystallogr. D52*, 623−630.

53. Ivankov, D. N., Garbuzynskiy, S. O., Alm, E., Plaxco, K. W., Baker, D., and Finkelstein, A. V. (2003) Contact order revisited: Influence of protein size on the folding rate, *Protein Sci. 12*, 2057−2062.
54. Semisotnov, G. V., Rodionova, N. A., Kutyshenko, V. P., Ebert, B., Blank, J., and Ptitsyn, O. B. (1987) Sequential mechanism of refolding of carbonic anhydrase B, *FEBS Lett. 224*, 9−13.
55. Semisotnov, G. V., Rodionova, N. A., Razgulyaev, O. I., Uversky, V. N., Gripas, A. F., and Gilmanshin, R. I. (1991) Study of the "molten globule" intermediate state in protein folding by a hydrophobic fluorescent probe, *Biopolymers 31*, 119−128.
56. Plaxco, K. W., Guijarro, J. I., Morton, C. J., Pitkeathly, M., Campbell, I. D., and Dobson, C. M. (1998) The folding kinetics and thermodynamics of the Fyn-SH3 domain, *Biochemistry 37*, 2529−2537.
57. Grantcharova, V., Alm, E. J., Baker, D., and Horwich, A. L. (2001) Mechanisms of protein folding, *Curr. Opin. Struct. Biol. 11*, 70−82.
58. Makarov, D. E., Keller, C. A., Plaxco, K. W., and Metiu, H. (2002) How the folding rate constant of simple, single-domain proteins depends on the number of native contacts, *Proc. Natl. Acad. Sci. U.S.A. 99*, 3535−3539.
59. Galzitskaya, O. V., Garbuzynskiy, S. O., Ivankov, D. N., and Finkelstein, A. V. (2003) Chain length is the main determinant of the folding rate for proteins with three-state folding kinetics, *Proteins 51*, 162−166.
60. Cobos, E. S., Filimonov, V. V., Vega, M. C., Mateo, P. L., Serrano, L., and Martinez, J. C. (2003) A thermodynamic and kinetic analysis of the folding pathway of an SH3 domain entropically stabilised by a redesigned hydrophobic core, *J. Mol. Biol. 328*, 221−233.
61. Sakurai, M., Moriyama, H., Onodera, K., Kadono, S., Numata, K., Hayashi, Y., Kawaguchi, J., Yamagishi, A., Oshima, T., and Tanaka, N. (1995) The crystal structure of thermostable mutants of chimeric 3-isopropylmalate dehydrogenase, 2T2M6T, *Protein Eng. 8*, 763−767.
62. Hirose, R., Suzuki, T., Moriyama, H., Sato, T., Yamagishi, A., Oshima, T., and Tanaka, N. (2001) Crystal structures of mutants of *Thermus thermophilus* IPMDH adapted to low temperatures, *Protein Eng. 14*, 81−84.
63. Numata, K., Hayashi-Iwasaki, Y., Kawaguchi, J., Sakurai, M., Moriyama, H., Tanaka, N., and Oshima, T. (2001) Thermostabilization of a chimeric enzyme by residue substitutions: Four amino acid residues in loop regions are responsible for the thermostability of *Thermus thermophilus* isopropylmalate dehydrogenase, *Biochim. Biophys. Acta 1545*, 174−183.
64. Suzuki, T., Yasugi, M., Arisaka, F., Oshima, T., and Yamagishi, A. (2002) Cold-adaptation mechanism of mutant enzymes of 3-isopropylmalate dehydrogenase from *Thermus thermophilus*, *Protein Eng. 15*, 471−476.
65. Watanabe, K., and Yamagishi, A. (2006) The effects of multiple ancestral residues on the *Thermus thermophilus* 3-isopropylmalate dehydrogenase, *FEBS Lett. 580*, 3867−3871.
66. Akanuma, S., Yamagishi, A., Tanaka, N., and Oshima, T. (1996) Spontaneous tandem sequence duplications reverse the thermal stability of carboxyl-terminal modified 3-isopropylmalate dehydrogenase, *J. Bacteriol. 178*, 6300−6304.
67. Nurachman, Z., Akanuma, S., Sato, T., Oshima, T., and Tanaka, N. (2000) Crystal structures of 3-isopropylmalate dehydrogenases with mutations at the C-terminus: Crystallographic analyses of structure-stability relationships, *Protein Eng. 13*, 253−258.
68. Kirino, H., Aoki, M., Aoshima, M., Hayashi, Y., Ohba, M., Yamagishi, A., Wakagi, T., and Oshima, T. (1994) Hydrophobic interaction at the subunit interface contributes to the thermostability of 3-isopropylmalate dehydrogenase from an extreme thermophile, *Thermus thermophilus*, *Eur. J. Biochem. 220*, 275−281.
69. Aoshima, M., and Oshima, T. (1997) Stabilization of *Escherichia coli* isopropylmalate dehydrogenase by single amino acid substitution, *Protein Eng. 10*, 249−254.
70. Akanuma, S., Yamagishi, A., Tanaka, N., and Oshima, T. (1999) Further improvement of the thermal stability of a partially stabilized *Bacillus subtilis* 3-isopropylmalate dehydrogenase variant by random and site-directed mutagenesis, *Eur. J. Biochem. 260*, 499−504.
71. Glyakina, A. V., Garbuzynskiy, S. O., Lobanov, M. Y., and Galzitskaya, O. V. (2007) Different packing of external residues can explain differences in the thermostability of proteins from thermophililic and mesophilic organisms, *Bioinformatics* (in press).
72. Szilágyi, A. N., and Vas, M. (1998) Sequential domain refolding of pig muscle 3-phosphoglycerate kinase: Kinetic analysis of reactivation, *Folding Des. 3*, 565−575.
73. Rhode, D. J., and Martin, B. L. (1999) Localized structural effects of electrostatic interactions in a thermostable enzyme, *Biochem. Biophys. Res. Commun. 258*, 179−183.
74. Miyazaki, K., Kadono, S., Sakurai, M., Moriyama, H., Tanaka, N., and Oshima, T. (1994) Chemical modification and site-directed mutagenesis of Tyr36 of 3-isopropylmalate dehydrogenase from *Thermus thermophilus* HB8, *Protein Eng. 7*, 99−102.
75. Onodera, K., Sakurai, M., Moriyama, H., Tanaka, N., Numata, K., Oshima, T., Sato, M., and Katsube, Y. (1994) Three-dimensional structures of chimeric enzymes between *Bacillus subtilis* and *Thermus thermophilus* 3-isopropylmalate dehydrogenases, *Protein Eng. 7*, 453−459.
76. Kotsuka, T., Akanuma, S., Tomuro, M., Yamagishi, A., and Oshima, T. (1996) Further stabilization of 3-isopropylmalate dehydrogenase of an extreme thermophile, *Thermus thermophilus*, by a suppressor mutation method, *J. Bacteriol. 178*, 723−727.
77. Qu, C., Akanuma, S., Tanaka, N., Moriyama, H., and Oshima, T. (2001) Design, X-ray crystallography, molecular modelling and thermal stability studies of mutant enzymes at site 172 of 3-isopropylmalate dehydrogenase from *Thermus thermophilus*, *Acta Crystallogr. D57*, 225−232.
78. Akanuma, S., Yamagishi, A., Tanaka, N., and Oshima, T. (1998) Serial increase in the thermal stability of 3-isopropylmalate dehydrogenase from *Bacillus subtilis* by experimental evolution, *Protein Sci. 7*, 698−705.

BI700754Q